A COMBINITORIAL APPROACH TO IDENTIFYING CANDIDATE MATERIALS FOR PHOTOCATALYTIC WATER SPLITTING

A Thesis

Presented to the Faculty of the Graduate School

Of Cornell University

In Partial Fulfillment of the Requirements for the Degree of

Masters of Science

by

Ian Fuller

May 2012

ABSTRACT

Combinatorial materials research can provide valuable insight into the relations between a materials composition, structure and properties of interest, especially when a broad understanding of these relations is lacking. Photocatalytic decomposition of water is one such research area in which the combinatorial process can be useful. The ability to synthesize and characterize many material combinations quickly and inexpensively can be very advantageous when properties of these combinations are unknown.

This thesis reports on the construction of a specialized electrochemical test cell designed to measure the photocatalytic properties of novel materials. The experimental setup utilizes various laser wavelengths and externally applied voltages to probe the effective band gap of the semiconductor materials. Furthermore, the results of this study clarify the techniques needed to identify a good photocatalyst and suggest improved experiments which could significantly expand on the current knowledge base.

BIOGRAPHICAL SKETCH

Ian Fuller was born in Cincinnati, Ohio but lived most of his life in Bellbrook, Ohio. He attended the Bellbrook school district and in the 6th grade, with the support of his parents and science teacher Mr. Douglass, participated in the school science fair. This started an annual tradition that, under the tutelage of his high school physics teacher, Mr. Carpenter, would take him to the International Science and Engineering Fair his senior year. It was at this event that he met the dean of the College of Engineering and Computer Science at a local university. Dr. Bor Jang persuaded Ian to attend Wright State University as an Engineering Physics major and also offered him an undergraduate intern position at his local research and development company. This internship took Ian through all four years of his undergraduate degree and opened his eyes to the wonder of new materials and how they could be used in real world applications.

Upon completion of his undergraduate degree, Ian decided to attend Cornell University in their Material Science and Engineering Master of Science program. While this was a large transition for Ian, having come from a local university near his family, it provided him with hands on experience in the equipment and processes of material science and allowed him access to experts in the materials science field. All of these experiences at Cornell have prepared Ian for the next stages of his life.

ACKNOWLEDGMENTS

This work was performed in part at the Cornell NanoScale Facility, a member of the National Nanotechnology Infrastructure Network, which is supported by the National Science Foundation (Grant ECS-0335765).

I would like to thank my graduate committee, Dr. Bruce van Dover and Dr. Héctor Abruña. They graciously provided their expertise, equipment, and time to help get this project off the ground and to the point it is today.

I would also like to thank the members of the van Dover research group for their support and help. Specifically, I would like to thank the other members of the photocatalytic research group past and present: Pauline Stewart, Bowen Dong, and Lin Xu for their support and patience as we repeatedly troubleshot the many issues that occurred throughout the building process. Without their ideas, persistence, and work this project would not be as far along as it is.

Finally, I would like to thank my wife Jackie and my family for their never ending support. I love you guys.

CONTENTS

LIST OF FIGURES

9. Photograph of the Fenris co-sputtering system along with portions of the control units.[19]
10. Chart of solar radiation intensity incident on the Earth's surface overlaid on the regions of the electromagnetic spectrum. Adapted from [13]
11. Example of semiconductor bandgaps and their valence and conduction band locations relative to the oxidation and reduction potentials of water.[14]
12. A cross-sectional view of the wafer sample. The SiO_2 insulating layer was made by baking the Si wafer in air at 1000 ^{o}C for three hours. The chrome layer was deposited by thermal evaporation, the platinum layer by e-beam evaporation, and the material spread by magnetron co-sputtering.
13. Schematic of electrochemical system for testing photocatalytic material spreads.
14. Photograph of experimental system. **A.** Z-Axis motorized stage. **B.** Electrochemical cell with Pt counter electrode, Ag/AgCl reference electrode, and material spread working electrode. **C.** Stanford Research Chopper. **D.** 532 nm diode laser. **E.** National Instruments PCI-6221 data acquisition card. Note that the potentiostat is not shown.
15. Schematic showing the process for determining current due to photocatalysis. **Step 1:** Compare measured current signal to chopper signal and split measured signal into a "light-on" and a "light-off" signal. **Step 2:** Average the two signals. **Step 3:** Subtract the averaged "light-off" signal from the averaged "light-on" signal to find the current due to the laser beam.
16. Front panel display of the LabVIEW program used for motor control and to measure the photo-response of the materials.

17. CV of a Pt WE in 0.1 M Na_2SO_4 solution. A stepped external potential was applied with a 25 mV sec^{-1} rate.
18. Color plot showing the absolute maximum current at each location when no material is present. Any resulting signal is due to electronic noise.
19. An example of the visual representations of the photocurrent data. LEFT: Color scale plot showing the absolute maximum current at each location as a function of wafer position. RIGHT: CV chart for a single wafer position showing the photocurrent as a function of the changing potential. In this example the -0.32 mA current at approximately -0.35 V would act as the "absolute maximum" current for this (x,z) location.
20. Photograph of Ti-Ni-Co wafer after 600 ^{o}C heat treatment for 3 hours.
21. Photographs of the Cu-Ni-Co oxide films. **A.** Film after deposition and air bake at 300 ^{o}C for 3 hours. **B.** Film after subsequent 450 ^{o}C air bake. **C.** Film after full wafer test run in 0.1 M Na_2SO_4.
22. Color plots of the Cu-Ni-Co oxide films. **A.** Results of the 405 nm test. The maximum wafer current of 7.3 μA was obtained at (16,52). **B.** Results of the 532 nm test. The maximum wafer current of 7.95 μA was obtained at (36,56).
23. Photographs of the Ta-Ni-Co oxide films. **A.** Film after deposition and air bake at 300 ^{o}C for 3 hours. **B.** Film after subsequent 450 ^{o}C air bake. **C.** Film after full wafer test run in 0.1M Na_2SO_4.

24. Figure 24: Color plots of the Ta-Ni-Co oxide films. **A.** Results of the 405 nm test. The maximum wafer current of 2 μA. **B.** Results of the 532 nm test. The maximum wafer current of 8.6 μA. Note the localized active areas of the 532 nm run.
25. Photographs of the Cu-Ti-Co oxide films. **A.** Film after deposition and air bake at 300 ^{o}C for 3 hours. **B.** Film after prolonged submersion in 0.1 M Na_2SO_4..
26. Photographs of the Cu-Fe-Ni oxide films. **A.** Film after deposition and air bake at 300 ^{o}C for 3 hours. **B.** Film after prolonged submersion in 0.1 M Na_2SO_4..
27. Photographs of the Cu-Ni-Ta oxide films after deposition, 300 ^{o}C air bake for 3 hours and electrochemical test run in 0.1 M Na_2SO_4.

LIST OF TABLES

LIST OF EQUATIONS

1. INTRODUCTION

Solar energy represents the single largest source of available energy on the planet. On average, 1.4 kW/m^2 of energy reaches the upper atmosphere and approximately 1.05 kW/m^2 of solar energy reaches the surface of the planet.[10] If even a fraction of this energy was able to be captured and utilized for energy applications, it could greatly change the energy landscape of the world. However, this is a very big IF. With that in mind, new methods of solar conversion, and more importantly solar energy storage, have been proposed. One such method involves using photocatalytic materials to split water into hydrogen and oxygen via the energy contained in sunlight.

The idea behind photocatalytic water splitting is illustrated in Figure 1, for a semiconductor that has conduction and valence bands (CB and VB respectively) located above and below the oxidation and reduction levels of water, respectively.[20] More precisely, such a material would have the CB level more negative than the redox potential of H^+/H_2 (0 V vs. normal hydrogen electrode), while the VB level must be more positive than the redox potential of O_2/H_2O (1.23 V vs. normal hydrogen electrode).[9] The difference between these two bands within the semiconductor represents the energy required to excite an electron from the conduction band into the valence band. In photocatalysis, this excitation is accomplished by the introduction of light with an energy greater than that of the materials band gap. Assuming a perfect photocatalyst, one that can take a photon of light and use it to create an electron-hole pair that can split water, light with an energy of just over 1.23 eV (1010 nm) will begin the

oxidation/reduction of water. For real world applications however, this energy must be greater than 1.23 eV in order to drive the the photocatalytic reaction at a reasonable and useful rate.

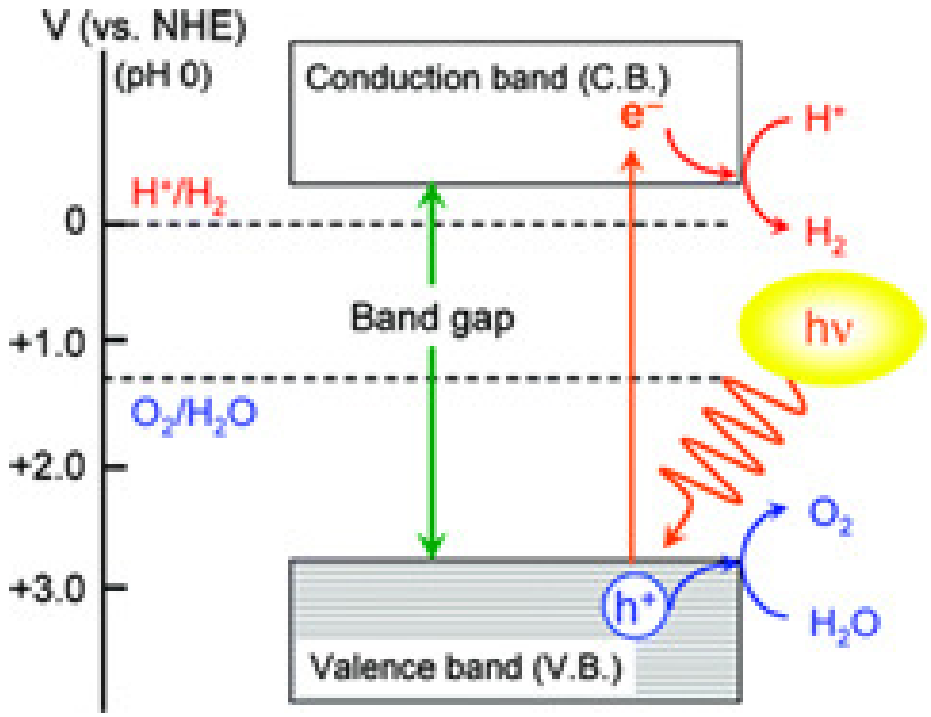

Figure 1: Diagram of a theoretical photocatalytic materials band gap relative to the oxidation/reduction potentials of water.[20]

1.1 State of the Art Photocatalytic Systems

Although TiO_2 pigments have been used since ancient times, the photo-assisted catalytic properties of the material were first observed by in 1972 by Japanese scientists Fujishima and Honda.[11] They found that when exposed to UV light, a TiO_2 electrochemical cell produced a current proportional to the intensity of the light source. The light needed to have a wavelength or less than 415 nm, or energy greater than 3 eV. This level was known to be the approximate band gap of the TiO_2 material. Furthermore, they showed that the current flowed from a Pt

electrode, through an external circuit and into the TiO_2 electrode. This direction suggests that the oxidation reaction (oxygen evolution) takes place at the TiO_2 surface while the reduction portion of the reaction was shown to occur at the Pt counter electrode.[11] While current was proportional to the intensity of the incident light, they noted that the kinetics of the reaction might increase if another material was discovered that worked on the reduction side of the reaction in the same way that TiO_2 works on the oxidation portion.

They showed one of the two main ways photocatalytic water splitting can occur. These two methods, the one-step and two-step systems, comprise the majority of active research on the topic. The two systems, as their names suggest, are differentiated by the number of materials needed to complete the oxidation and reduction of the water. Figure 2 illustrates two different methods of splitting water using known photocatalytic materials.[12]

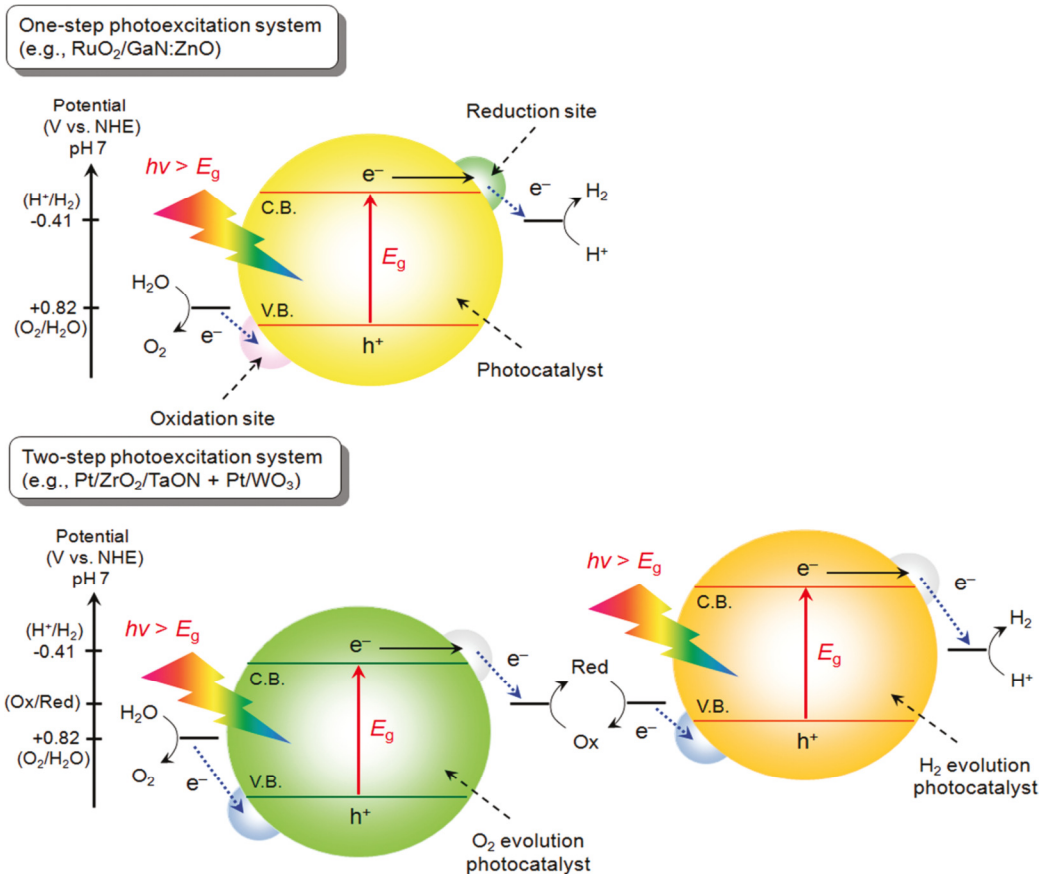

Figure 2: Diagram displaying two different methods for creating photocatalyst systems. The top diagram shows the one-step system wherein one material does both the oxidation and reduction of the water. The lower system displays the two-step approach that utilizes two individual materials, one for reduction and one for oxidation.[12]

Both methods have their strengths and weaknesses. While the one-step system only requires the use of a single material capable of photocatalysis, the energy of light must be greater than the decomposition potential of water. In actuality the photon energy needs to be significantly larger than the 1.23 eV of water in order to drive the reaction at a sufficient rate. On the other hand, the two-material system is not restricted by this decomposition potential. As long as the conduction band of one material and the valence band of the other are in the correct locations with respect to the potential for hydrogen and oxygen evolution, the

wavelength of the light can be minimized to just above the larger of the gaps of the two materials. This theoretically could allow a much greater percentage of the solar spectrum to be utilized. However, the increased efficiency is accompanied by increased system complexity and the need to discover two materials that are sufficiently photoactive.

There are many possible material combinations for visible light photocatalysts, so it is useful to attempt to classify groups of materials that may behave in similar ways in order to rationally guide the choice of material combinations. We limit our discussion to oxides, since these materials are most likely to exhibit the chemical stability in aqueous solutions. For this purpose, elements from the periodic table can be broken down into different categories:[14][15]

- Ionic charge compensators that may help to construct complex crystal structures such as perovskites, pyrochlores, and spinels
- Catalytic materials that may help to lower the overpotential losses of the reaction
- Structural materials that provide stable, high heat of formation, oxides
- Light absorbing materials to utilize the widest range of the solar spectrum

While this categorization is not all encompassing and there are exceptions to every rule, it does provide a framework from which to begin combining materials for effective photocatalysts. A good starting point would be to combine materials from different categories in order to form a material that meets all the requirements of water splitting. This process may be simplified by choosing materials that can qualify in more than one of the categories.

Materials such as NiO_x and CoO_x have shown possible light absorbing properties as well as catalytic properties.[15] A quick visual reference can be built to provide a basis for photocatalytic combinations. When overlaid on a periodic table it provides the needed categories readily (See Figure 3).[14][15][24]

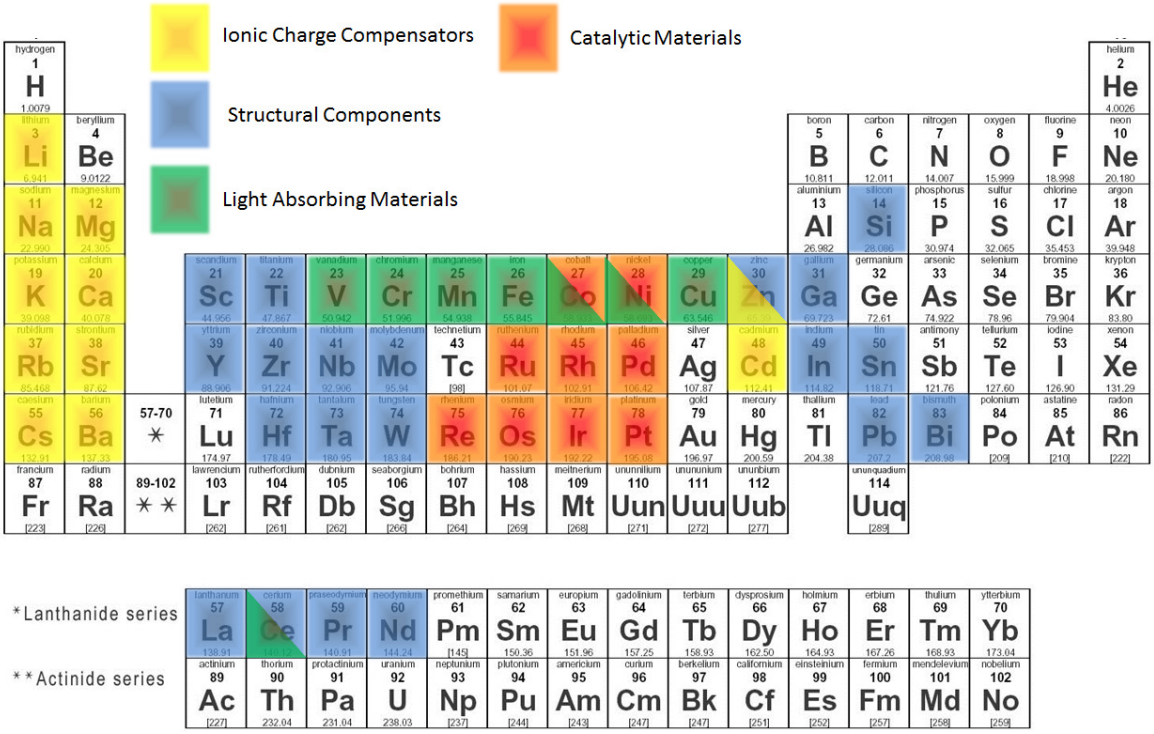

Figure 3: Periodic table with color coded elements representing possible roles in future photocatalytic water splitting materials. [14][15][24]

As stated earlier, while not definitive, this table provides a framework for starting photocatalytic research. Some materials, such as Cd and Pb may be unusable due to their toxicity while others such as the alkali metals may be difficult to work with in their metallic form.

Defining the current "best" photocatalyst involves some ambiguity. As the properties of the materials are different from one another, several factors are needed to compare different systems. These factors include the quantum yield, the maximum wavelength under which the system is active, and whether or not any sacrificial reactants (materials that increase overall activity but need to be replenished after a period of time) are necessary for the reaction to proceed. The last of these is highly undesired as it greatly reduces the usefulness in real world applications. The quantum yield can be defined as:

$$QY\ (\%) = \frac{Number\ of\ reacted\ electrons}{Number\ of\ incident\ photons} x\ 100\%\ ^{[14]} \quad (1)$$

Once a material combination has shown photocatalytic properties it is necessary to draw comparisons and set benchmark levels of activity. An overall target efficiency can be defined as a quantum yield of around 30% at a minimum wavelength of 600nm (2eV).[9] Such an overall system has yet to be discovered but certain material combinations have been shown to meet at least one of these qualifications.

Photocatalytic materials such as NiO/$NaTaO_3$:La have shown to have extremely high quantum yields, approaching 56% and do not require sacrificial reagents. But this photocatalytic material requires high-energy UV photons, at least 4.59 eV (i.e., $\lambda < 270$ nm); this is a far higher energy than the desired value.[14] ZnS provided an even higher quantum yield of 90% at 313 nm but requires a reaction solution of $Na_2S + H_3PO_2 + NaOH$ to act as an electron donor.[14] $(Ga_{0.88}Zn_{0.12})(N_{0.88}O_{0.12})$ has shown photocatalytic activity in the relatively long

wavelength range of 420-440 nm, and does not require support by sacrificial materials. However, the quantum yield is only 5.9%.[14]

In general, the bandgap requirement has been the hardest to satisfy. Photocatalysts that can operate using visible light have been difficult to create due to the relatively small bandgap inherent in these oxides.

Several routes exist in the search for novel materials for visible light photocatalysis. One promising approach involves searching transition metal oxide combinations for compounds that have yet to be evaluated. As this process, by its very nature, involves many thousands of unique material combinations, a high-throughput method of creating and testing these materials is highly desirable. A method using inkjet printing was employed by Parkinson et.al.[15], who synthesized ternary spreads of materials utilizing oxides of copper, iron, caesium, and neodymium. These materials were arranged in a triangular array as seen in Figure 4.

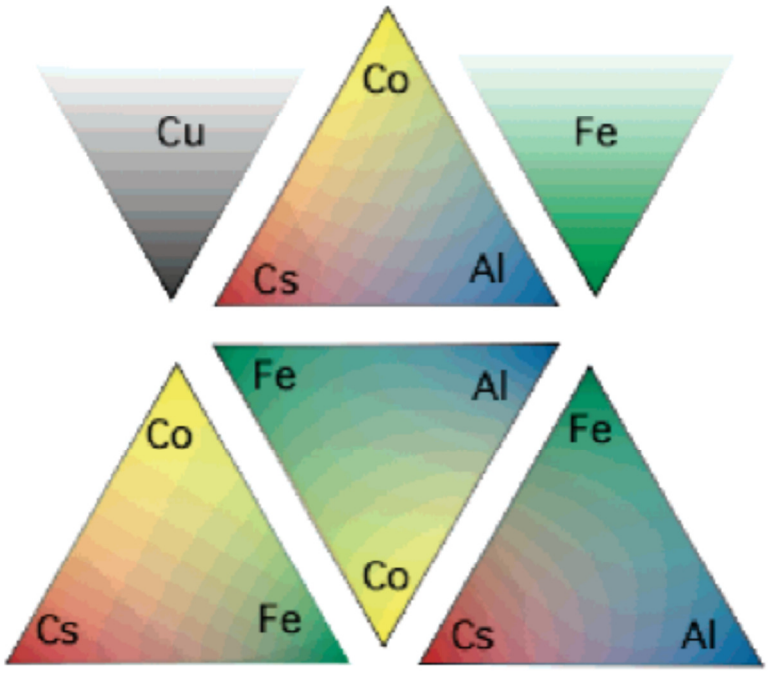

Figure 4: Schematic of the ternary spread triangles used to test the photocatalytic properties of certain materials. Note the pure copper and iron triangles in the upper left and right corners. [15]

The material spreads were deposited on fluorine-doped tin oxide coated glass and then irradiated with light of (514.5 nm, 532 nm, or 632.8 nm) in a solution of 0.5 M NaOH. The laser beam was moved over the samples and the resulting photocurrent was measured at each distinct location. Furthermore, they applied an external voltage between -0.5 V and +0.5 V at each location to ascertain whether the material is acting to oxidize the water (photocurrent produced under a positive external bias) or to reduce the water (photocurrent observable under a negative external bias).[15] By changing the potential it is possible to determine whether the materials are light absorbing but require an external bias to drive the reaction. Some results of this experiment are shown in Figure 5.

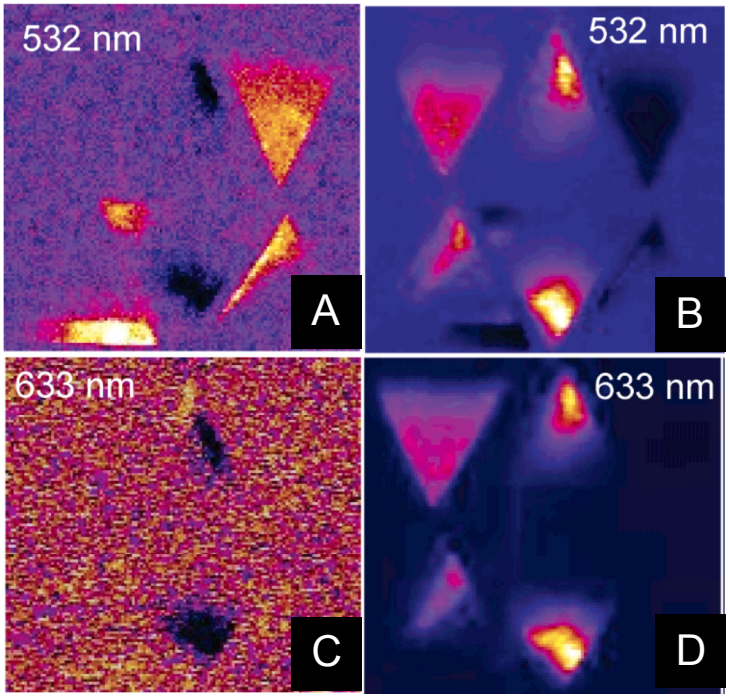

Figure 5: Laser scans of samples shown in Figure 4 (Above picture). **A.** Scan with 532 nm with 0.5 V bias in 0.5 M NaOH solution. **B.** Same laser scan with an external voltage of -0.5 V. **C.** Same laser scan with 633 nm laser and 0.5 V bias. **D.** Same laser scan with 633nm laser and -0.5 V bias.[15]

Other research has focused on attempting to alter the band gap of known UV-active photocatalysts to an energy level more suitable for visible light water splitting. This is typically accomplished through either a chemical or physical process. In the first case, the band gap is decreased by some chemical modification such as the addition of a dopant material. One such technique involves the addition of nitrogen into the oxide to form an oxynitride. Nitrogen incorporation can form an impurity energy band above that of the oxygen 2p band.[16] The raised valence band results in a lower effective band-gap. While the magnitude of the change is dependent on many factors it can have a significant effect on the bandgap of oxide materials. For example, ZnO has a bulk band gap of 3.27 eV.[16] However, samples of ZnO doped with nitrogen and grown at 25^{o}C have been shown to exhibit a band gap of 1.75 eV, corresponding

to a visible light wavelength of 708 nm. This effect of nitrogen incorporation is well-established in theory and experiment. Computational studies have shown that the presence of Hf_3N_4 in a HfO_2 material also works to lower the band gap (4.06 eV for HfO_2 vs. 2.51 eV for $(HfO_2)_3(Hf_3N_4)$).[17] Finally, experimental work has found similar results for both copper and nickel oxynitrides (See Figure 6).[18]

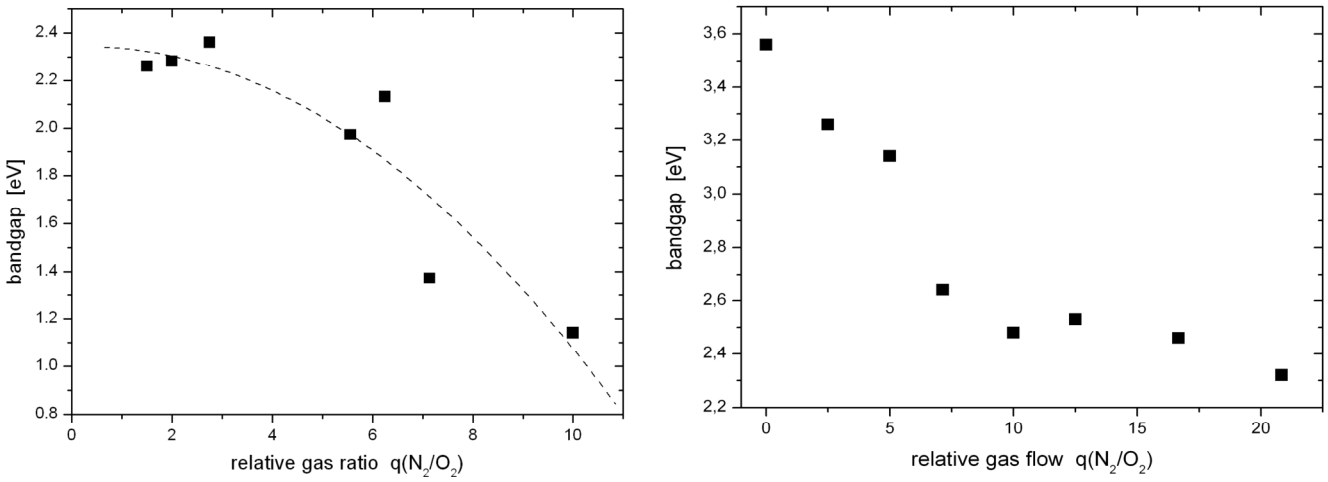

Figure 6: Effect of nitrogen incorporation on the bandgaps of copper oxide (LEFT) and nickel oxide (RIGHT).[18]

It is with this background information that this research attempts to shed light on the requirements necessary to achieve a one step, visible light photocatalyst that can act as a solar energy conversion device.

2. BACKGROUND INFORMATION

2.1 90^{o} Off-Axis Reactive RF Magnetron Co-Sputtering

The term sputtering is used to define a physical vapor deposition (PVD) technique in which atoms are ejected from the surface of a target material when struck by other energetic particles. This deposition technique is able to provide a level of composition control extremely suitable for preparing material composition spreads.[21] Typically, sputter systems operate at higher pressures than evaporation systems, which increases the possibility of incorporation of contaminants. Since the background gasses in high-vacuum systems are typically dominated by H_2O this contamination usually has little effect on the growth or properties of oxides, though it may be problematic for preparation of clean materials.

2.1.1 Sputtering System

The basic operation of a sputtering system involves creating a plasma of positively charged ions of an inert gas, typically argon, and accelerating them toward a material target. Those ions bombard the surface of the target and cause target atoms to be dislodged from the surface. These sputtered atoms impinge on the substrate and condense to form a thin film of the desired material.[21] A schematic of this process can be seen in Figure 7. A magnetic field created behind the target material is used to increase the probability that secondary electrons from the target will ionize the Ar atoms, thereby creating a self-sustaining plasma.

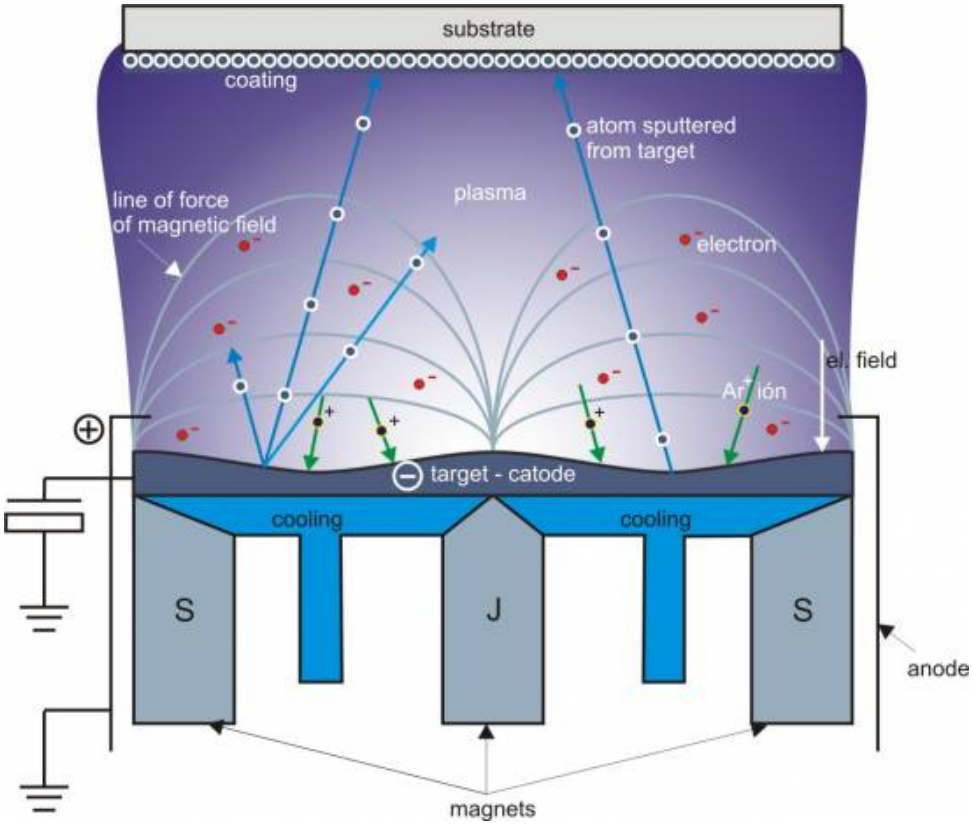

Figure 7: Schematic of the internal workings of a magnetron sputtering gun. [22]

While this basic operation is simple, variations on the technique can be employed to garner a wide range of results. In the case of this study, a sputtering variation was employed to provide a reproducible, high-throughput ternary material spread. This variation, known as 90° Off-Axis Reactive RF Magnetron Co-Sputtering, utilizes sputter targets arranged on a level above the substrate and perpendicular to the plane of the substrate. Multiple guns can be included and may be independently controlled enabling simultaneous deposition from multiple targets.[19] While argon is often used as the inert gas, reactive species can be introduced as well. Such gases, typically oxygen, are regulated using a mass flow controller in order to precisely define the percentage of reactive gas in the reaction chamber. However, the addition of these

reactive gases introduces issues for traditional sputter systems. As reactive gases such as oxygen or nitrogen form negative ions, they are repelled by the negative bias of the target. In 90^{o} off-axis sputtering, the fact that the guns do not point at the target reduces the excessive bombardment introduced by these ions. Finally, the RF portion of the sputtering technique refers to the fact that AC power is applied to the cathode of the sputter system. In a DC setup, only conductive films may be deposited as insulating or semiconducting targets accumulate charge that compensate the cathode potential.

The specific sputter system used in this study employs the 90^{o} Off-Axis Reactive RF Magnetron Co-Sputtering configuration. The system utilizes three, three-inch guns that are arranged at 90^{o} intervals on a circle parallel to the plane of the substrate. This setup, as illustrated in Figure 8 allows simultaneous deposition of up to three different materials (typically elements). The arrangement of the guns allows material gradients to be created with a high concentration near the gun that decays across the substrate. Although the gradient depends on the materials and system specifications, a typical value is approximately 1 at.% per mm. By utilizing three guns it is possible to create a material spread that includes a 1:1:1 material ratio at the center of the wafer. These ratios can be altered as desired depending on the properties of the target materials and the power of the sputter guns.

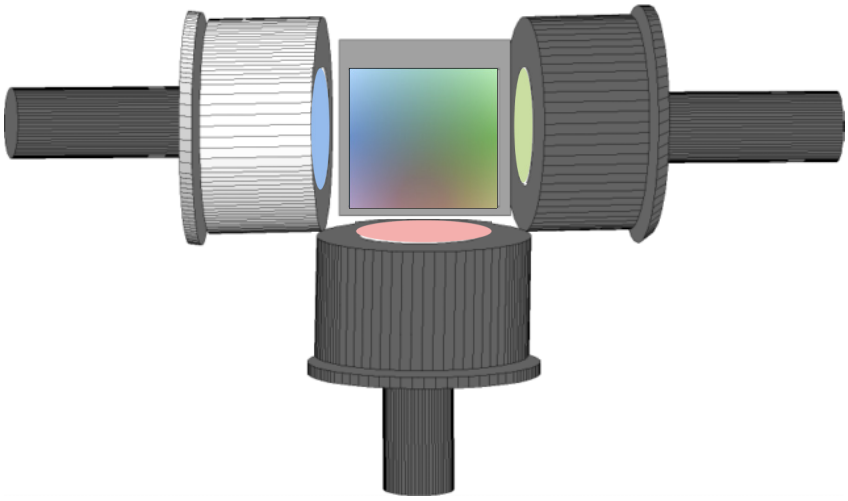

Figure 8: Schematic showing the orientation of a three gun co-sputtering system. Note the color of each gun and the resultant material spread on the center wafer. [19]

2.1.2 Fenris Specifications

The sputtering system utilized in this study, known as “Fenris”, is an example of an RF magnetron sputtering system capable of both on- and off-axis sputtering (see Figure 9). It specifically utilizes three Angstrom Onyx-2 magnetron guns incorporating two-inch targets. Argon is used as the inert gas while oxygen and nitrogen flows are controlled by MKS mass flow controllers. Fenris includes a wafer heater in order to allow substrates to be maintained at elevated temperatures, up to 300 ^{o}C, during sputtering.

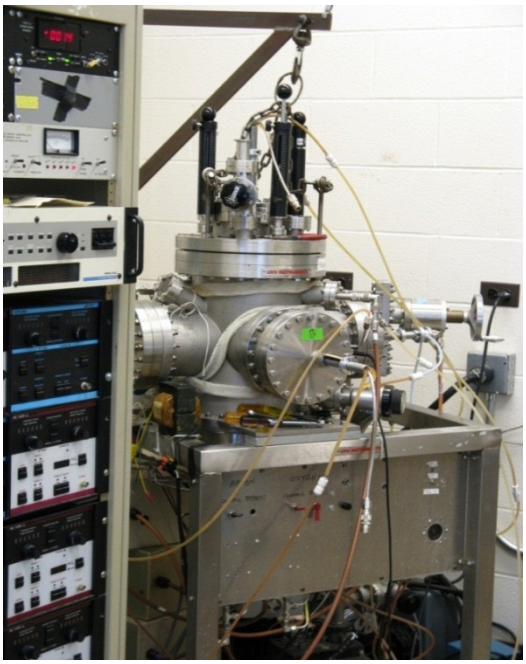

Figure 9: Photograph of the Fenris co-sputtering system along with portions of the control units. [19]

2.2 Photocatalytic Factors of Merit

1. Electronic Band Gap

In order for a material to be a viable candidate for photocatalysis it must possess a band gap which would allow solar radiation to excite a given electron from the valence band of the material to the conduction band. While materials have been found (reference TiO2) to be suitable photocatalytic water splitters they often possess band gaps greater than 3.1 eV. Such energies fall within the ultraviolet region of the electromagnetic spectrum and therefore are not suitable for solar spectrum absorption (See Figure 10). An ideal band gap for solar spectrum photocatalysis would harness the maximum amount of light within the highest intensity region of the visible spectrum

(approximately 1.65-2.6 eV). As any photon with energy greater than the band gap will excite the electrons within the material, the higher efficiency systems will possess band gaps that are as low as possible. For example, a material with a 3.1 eV band gap will be able to theoretically harness only 5% of the energy available in solar radiation whereas one with a 1.7 eV band gap has a theoretical maximum absorption of approximately 51% of the available energy of solar radiation at sea level.

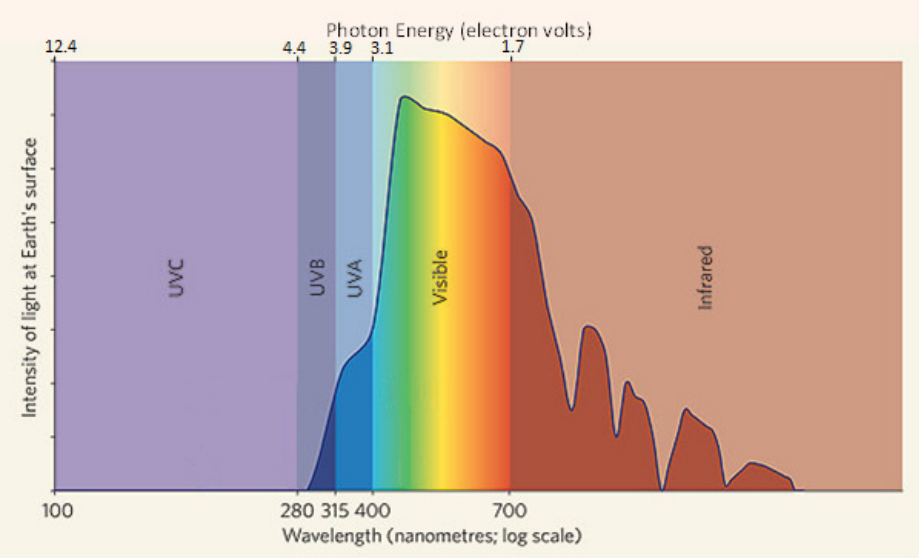

Figure 10: Chart of solar radiation intensity incident on the Earth's surface overlaid on the regions of the electromagnetic spectrum. Adapted from [13]

2. Valence and Conduction Band Locations

While the overall band gap of the material is important to determine a theoretical efficiency based on the solar spectrum, it is also necessary to look at the location of the conduction and valence bands and compare them to the oxidation and reduction potentials of water. In order to effectively split water the materials CB and VB locations should be close to, but slightly offset from these potentials. In particular, the

materials valence band should be located higher than the oxygen oxidation potential and the materials conduction band should be lower than the hydrogen reduction potential.[6] As water splitting has a minimum energy of 1.23 eV, this implies the minimum energy bandgap that a potential photocatalyst must possess.[8] While 1.23 eV is the theoretical minimum photon energy, it is necessary to overshoot this target in order to drive the reactions at rates suitable for practical applications. Some common semiconductor band locations relative to the oxidation and reduction potentials of water are shown in Figure 11.[14]

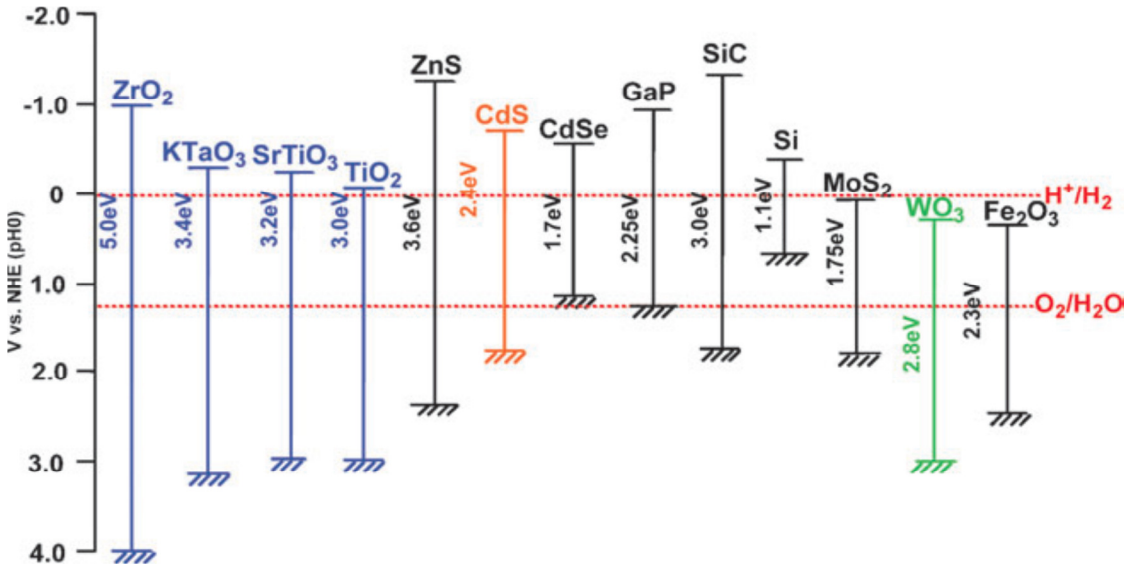

Figure 11: Example of semiconductor bandgaps and their valence and conduction band locations relative to the oxidation and reduction potentials of water.[14]

3. Material Stability

Even if the aforementioned items are addressed the material in question must be able to maintain its chemical and physical integrity for long periods under varying pH environments. As pure water is non-conducting, electrolytes are needed to support two-

electrode reactions; solutions typically incorporate sodium sulfate (Na_2SO_4), sodium hydroxide (NaOH), potassium hydroxide (KOH), sulfuric acid (H_2SO_4), or magnesium sulfate ($MgSO_4$). Any suitable photocatalyst would need to be stable under these environments at temperatures approaching 100 ^{o}C. These materials, as well as any other "balance-of-systems" components must maintain efficiency under continuous operation for many years in order to provide a market-ready replacement for current PV technology.

4. Electronic Recombination and Optical Absorption

Electronic recombination and optical absorption concerns the way electrons and photons interact within the material. Primarily the material needs to have an absorption length less than the physical depth dimension of the photocatalyst. If the absorption length is greater than that of its physical size, a portion of the photons will proceed through the material without creating an electron-hole pair. Materials with a large absorption length must be proportionally thicker than materials with a short absorption length.

Secondly, electron-hole recombination length must be as long as possible in order to allow the electron-hole pair to reach the surface of the material and react with the water. As this length is typically short (on the order of tens to hundreds of nanometers depending on material characteristics and crystallinity) it is advantageous to keep the material sample as thin as possible in order to allow the maximum number

of electrons and holes to interact with the outside water. Thus it is desirable to find a material that combines a short absorption length with a long recombination length.

5. Material Economics and Availability

As with any material-based technology, thought must be given to the availability and accessibility of the materials in question, and this is true for possible novel material combinations for photocatalytic water splitting. While some rare earth materials such as platinum and iridium are known to offer high catalytic activities, the sheer volume/cost of material that would be needed negates the possibility of using most of these precious or rare materials. The only exception is when the rare earth materials are used as dopants in minute quantities compared to the host material.

2.3 Research Goals

All of these quality metrics, along with previous research, must be taken into account when designing a high-throughput test station for evaluating photocatalytic materials, as well as determining the priority with which material combinations should be tested. With all of this information in mind an experimental setup was designed and built to provide information and guidance for future photocatalytic research. The test station is designed to measure photocatalytic current of novel material combinations and rapidly determine trends in activity, so that an efficient feedback loop can be run. The photo-current is used as a substitute for the direct measurement of evolved gas species. It is much easier and more reliable to measure the

current associated with illumination of a small region of photocatalytic material compared to attempting to measure the direct evolution of hydrogen and oxygen gas.

3. EXPERIMENTAL SETUP

The photocatalyst measurement setup is designed to analyze up to thousands of material combinations per combinatorial wafer. An electrochemical cell allows a cyclic voltamagram to be created based on an applied external voltage and the photo-current from the sample. By comparing the photocurrent, laser wavelength, and applied voltage, insights may be revealed into the workings of photocatalytic materials. This setup utilizes two, BCS150 stepper motors from Thorlabs, Inc. as well as an SR540 optical chopper from Stanford Research Systems. The electrical measurements were taken with a PINE AFRDE5 bi-potentiostat with the output digitized using a National Instruments, PCI-6227 37-pin multifunction DAQ. The functioning of all these devices is controlled by programs written using National Instruments LabVIEW 11.

3.1 Wafer Preparation

The thin film composition spreads are prepared by 90^{o} off-axis reactive magnetron co-sputtering onto a 3 inch diameter, single crystal Si wafer. The sputtering system allows three materials to be deposited simultaneously with areas of high material concentration near each respective gun and typically area of 1:1:1 composition at the middle of the wafer. This ternary spread will allow information to be gained based solely on the different material combinations, eliminating run-to-run variations that can confound single-composition studies. Furthermore,

sputtering the samples allows for various deposition parameters to be explored including overall pressure, oxygen partial pressure, nitrogen partial pressure, and substrate temperature. This provides a wide range of tools for material optimization.

Pretreatment of the wafer prior to sputtering is necessary in order to provide a highly conductive underlayer needed for photocurrent experiments. Silicon wafers (<100> orientation) from University Wafers were baked in air at 1000 ^{o}C for three hours and then cooled at a rate of 100^{o} per hour. This allows a layer of SiO_2, approximately 11 nm thick to be created on the wafer.[23] This oxide layer acts as an insulator preventing the Si from interacting chemically with the Cr and the Pt subsequently deposited. It also prevents any spurious current from the back side of the wafer in the electrochemical cell. Equipment at Cornell NanoScale Science and Technology Facility (CNF) was used to perform thermal and e-beam evaporation of the platinum conducting layer and the necessary chrome sticking layer. Thermal evaporation was used to initially deposit the 10 nm layer of chrome before a 25 nm layer of platinum was deposited using the electron beam system. The overall cross-sectional layout of the wafer is shown below in Figure 12.

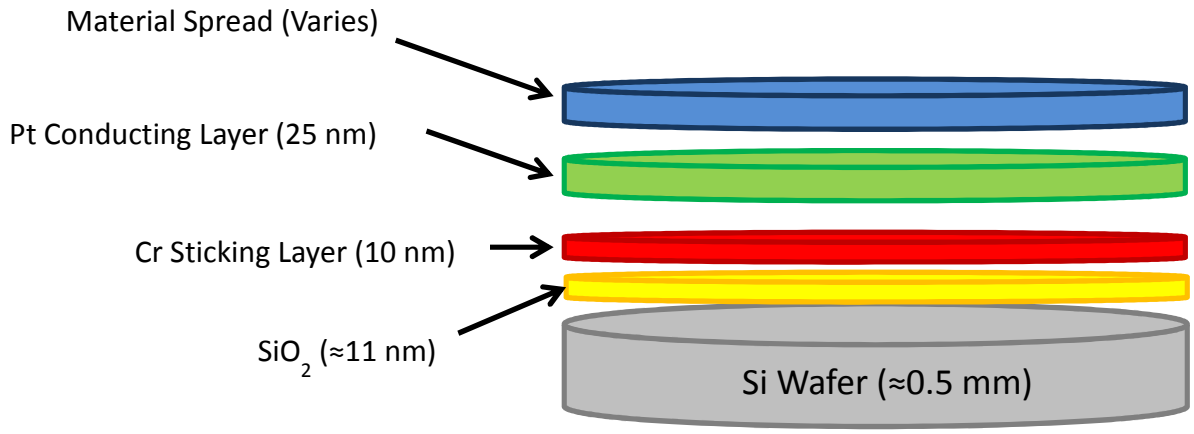

Figure 12: A cross-sectional view of the wafer sample. The SiO_2 insulating layer was made by baking the Si wafer in air at 1000 ^{o}C for three hours. The chrome layer was deposited by thermal evaporation, the platinum layer by e-beam evaporation, and the material spread by magnetron co-sputtering.

After the evaporation and sputtering processes were completed, visual observations were taken to record the "pre-test" condition of the wafer. These observations noted any surface roughness, any peeling of the thin film, as well as the level of oxidation. The qualitative level of oxidation was determined by observing the interference colors created by the transparent oxide films. Visual observation was repeated after any subsequent heat treatments as well as after the first test run in the electrochemical cell.

3.2 Electrochemical and Mechanical Setup

After the thin film is photographed, the wafer is immersed into the electrochemical cell along with an Ag/AgCl reference electrode and a 7 in^2 platinum counter-electrode. A rectangular glass container is used in order to provide a short and direct path from the laser to the sample. Originally, the electrolyte solution was a 0.5 M NaOH solution. This high pH solution (13.7) works to shift the HOMO and LUMO levels of water with respect to the oxide

band structure. However, as cyclic voltammetry allows arbitrary shifting of the potential of the electrolyte, indirect observation of the band gap it is not necessary to shift the conduction band in order to observe photocatalytic results. With this in mind, a 0.1 M $NaSO_4$ was used instead as this provides a much more neutral, non-corrosive environment that would be much easier to replicate in a real-world, energy producing scenario.

The 3" composition-spread sample functions as the working electrode in the electrochemical cell. All three electrodes are electrically connected to the potentiostat which controls the electrochemical measurements and offset voltages. The photocurrent measurements are then read out of the potentiostat and into the National Instruments data acquisition card. This card then communicates directly with the LabVIEW control program.

The material sample is attached to two, Thorlabs 150mm linear motorized stages that provide an X-Z framework in order to move the sample within the container. By moving the sample with respect to the light source we are able to probe every point on the surface with the highest simplicity and uniformity. The two motorized stages are controlled by the Thorlabs BSC102 stepper motor controller which provides an ActiveX interface for the LabVIEW control program. A schematic of the electrochemical and mechanical setup is shown in Figure 13 while the actual experimental system can be seen in Figure 14.

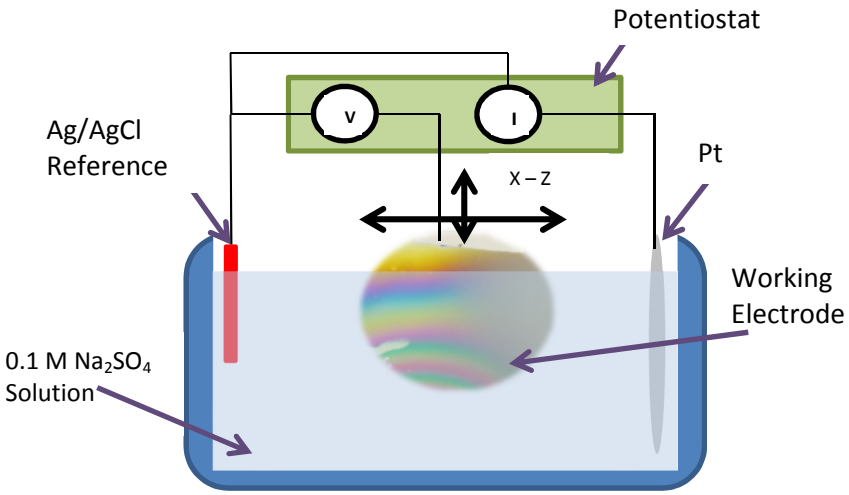

Figure 13: Schematic of electrochemical system for testing photocatalytic material spreads.

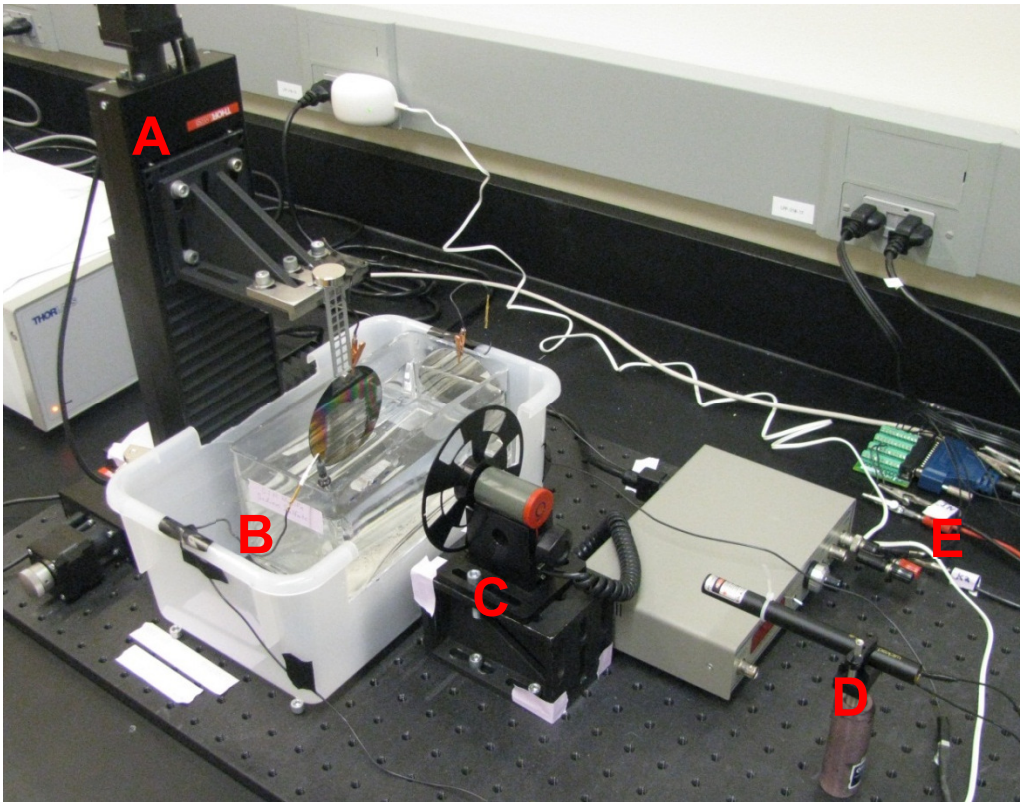

Figure 14: Photograph of experimental system. **A.** Z-Axis motorized stage. **B.** Electrochemical cell with Pt counter electrode, Ag/AgCl reference electrode, and material spread working electrode. **C.** Stanford Research Chopper. **D.** 532 nm diode laser. **E.** National Instruments PCI-6221 data acquisition card. Note that the potentiostat is not shown.

In order to better isolate the photocurrent signal due to our lasers from that of any outside noise or light source a Stanford Research Chopper was employed in front of the sample and electrolyte solution.[4] By chopping the light source at 13 Hz it is possible to observe the light on vs. light off current from the sample at any potential. This is accomplished by comparing a 0-5 V chopper signal to the photocurrent signal. The light-on signal is then subtracted from the light-off signal to provide an accurate representation of the photocurrent due to the incident laser (See Figure 15). Although the entire experimental setup is placed in an opaque enclosure, the addition of the chopper function provides a very good way to eliminate the effect of background light as well as any parasitic current conducted by un-illuminated portions of the working electrode. While the chopper frequency is 13 Hz, data on the sample photocurrent is taken at a higher sampling frequency (13 kHz) in order to provide maximum averaging to achieve a good signal to noise (SNR) ratio.

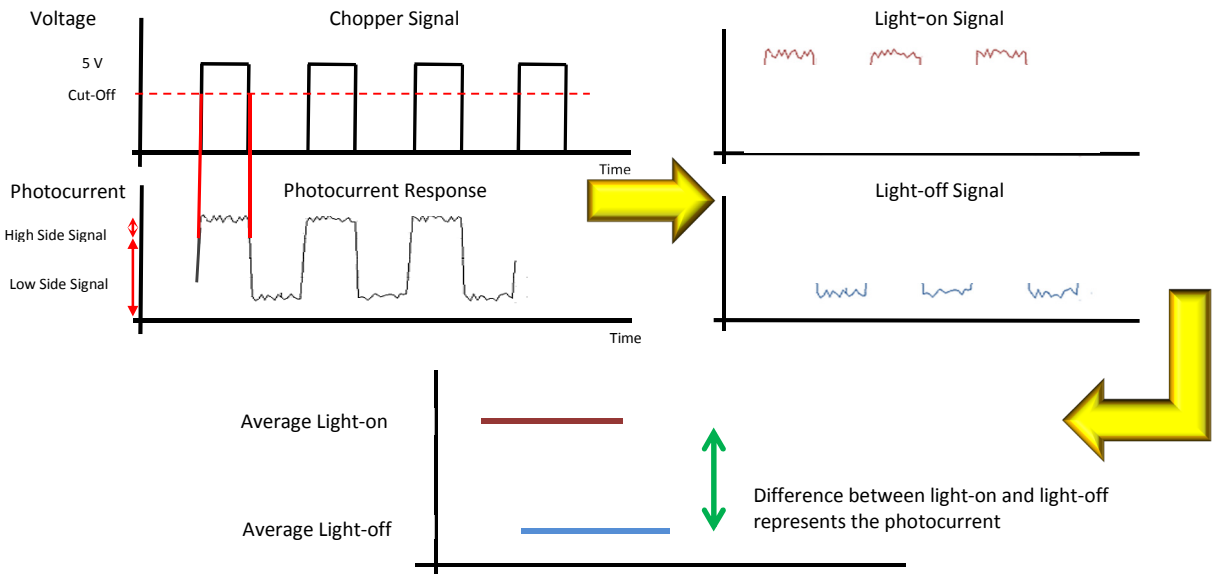

Figure 15: Schematic showing the process for determining current due to photocatalysis. **Step 1:** Compare measured current signal to chopper signal and split measured signal into a "light-on" and a "light-off" signal. **Step 2:** Average the two signals. **Step 3:** Subtract the averaged "light-off" signal from the averaged "light-on" signal to find the current due to the laser beam.

Finally, three lasers were available for the illumination source and were interchanged to provide information on the photocatalytic responses and electronic properties of the materials. The first laser is a 1 mW, 632.8 nm He-Ne laser from Metrologic. The other two lasers are a 5 mW, 532 nm core series laser and a 25 mW, 405 nm E2 series laser from Wicked Lasers.[3] These three lasers provide a photon energy range from 1.96 eV to 3.07 eV. This range of energy allows for the possibility of greater understanding of the behavior of the material and its relation to the band gap.

3.3 LabVIEW Pseudo-code

1. Move X-axis stage to specified X position
2. Move Z-axis stage to specified Z position
3. Output desired voltage offset to electrochemical cell
4. Measure photocurrent from sample for period of time via potentiostat
5. Average on-state signal and off-state signal
6. Subtract “on-state” response from “off-state” response
7. Record x position, z position, offset voltage, and photo-response current
8. Repeat steps 3-7 for different offset voltages
9. Repeat steps 1-8 for different X and Z positions
10. Observe the photocurrent based on wafer position and offset voltage

The LabVIEW program uses the current National Instruments DAQ-MX drivers to communicate with the PCI-6227 DAQ. A Thorlab’s active-X sub-VI, APT User, is also used within the LabVIEW program to communicate with the BSC102 stepper motor controller box. The maximum theoretical current based on the power and wavelength of the utilized laser is also calculated on the front panel (assuming 100% quantum efficiency and perfect catalytic efficience). This front panel of the test program can be seen in Figure 16.

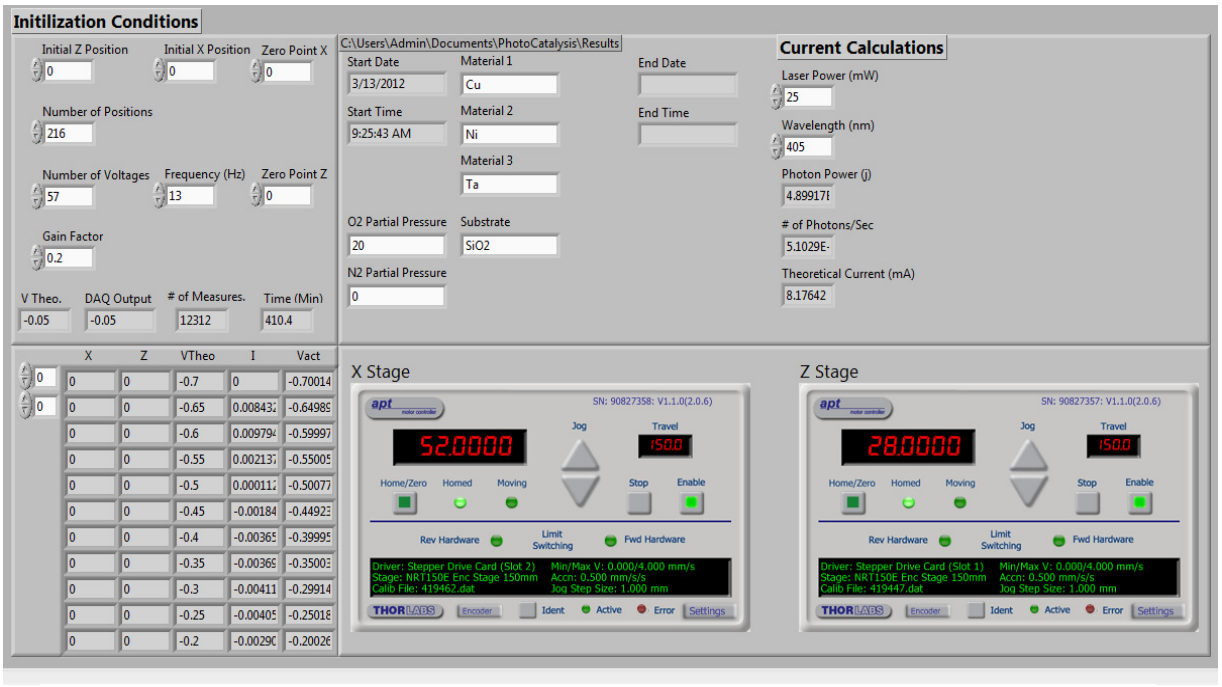

Figure 16: Front panel display of the LabVIEW program used for motor control and to measure the photo-response of the materials.

The output of this LabVIEW program is a text file containing the array shown in the lower left-hand corner of the front panel. This array contains the X and Z location data as well as the photocurrent, the desired offset voltage, and the measured offset voltage. Independent programs are available to display the results of the test runs. These programs display the CV curves at each location as well as the photocurrent as a function of wafer position.

3.4 Verification of Experimental Setup

Before testing on novel materials could proceed, it was necessary to determine the working characteristics of the experimental setup. This process began by verifying the relationship between the chopper and the electrical and software systems. This was achieved by using a small photovoltaic cell and activating it using the chopped laser system. This allowed

the software responsible for the on-off voltage measurements to be optimized. It was found that the voltage measurement was optimized by increasing the frequency of measurements while leaving the chopper at 13 Hz. This increase in sampling rate from 260 Hz to 13 kHz increased the signal-to-noise ratio and improved the visibility of the photocurrent signal. After verifying that the program produced results consistent with a PV cell the next step involved implementing the electrochemical system.

The electrochemical system is inherently more complicated than the mechanical system. Initially, a thin film platinum sample was used to confirm the electrochemical operation of the system. The platinum working electrode was chosen in order to provide a conductive yet inert system to check only the electrochemical system without the laser system. For this verification, the platinum working electrode was submerged in the 0.1 M Na_2SO_4 solution whose potential was stepped -0.3 to 1.2 V in 25 mV increments, one step per second. A total of 13,000 current measurements were taken at each potential. This scan was performed five times as shown in Figure 17. This CV suggested a Pt film but with impurities on the surface.

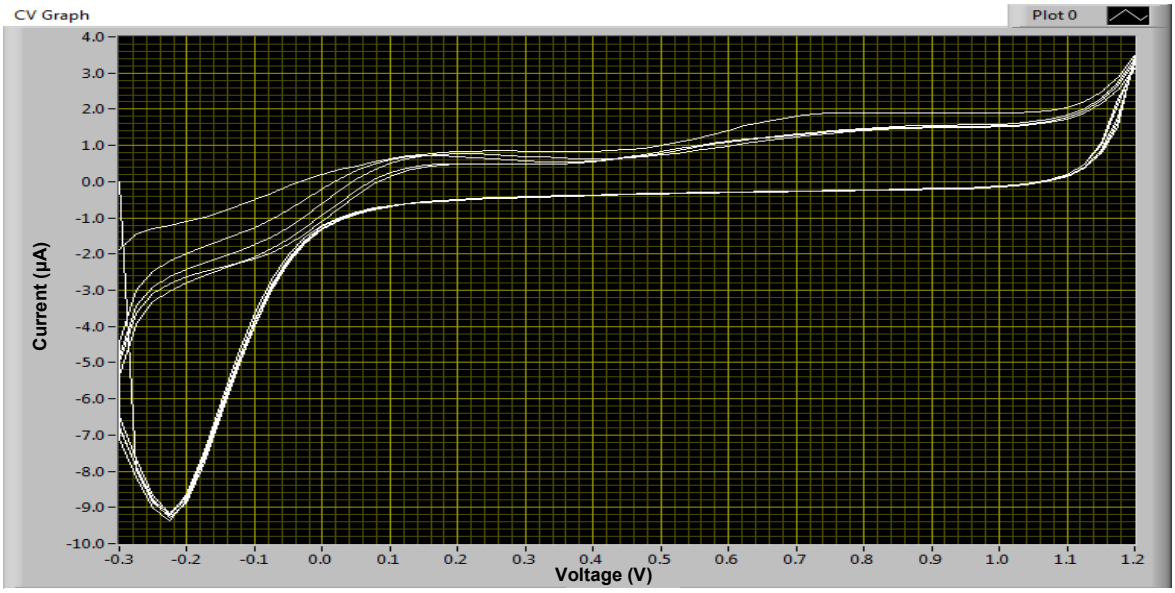

Figure 17: CV of a Pt WE in 0.1 M Na_2SO_4 solution. A stepped external potential was applied with a 25 mV sec^{-1} rate.

Finally, a simultaneous test of the mechanical and electrochemical system was performed by observing the photocurrent response when no material is present. To accomplish this, a thin Pt foil was used as the working electrode solely to provide the electrical connection to the solution. The foil was positioned such that the laser beam would never be incident on it. This provided a signal that should be due to system noise only. The X and Z stages were moved by 4 mm increments in order to scan a wide range quickly. The resulting color plot (Figure 18) displays the results of this test. It can be seen that the resulting signal is very small with an average signal of approximately 30 nA. Although this baseline noise signal should be dependent on the material acting as the working electrode, this test provided an idea of the magnitude of the underlying noise signal.

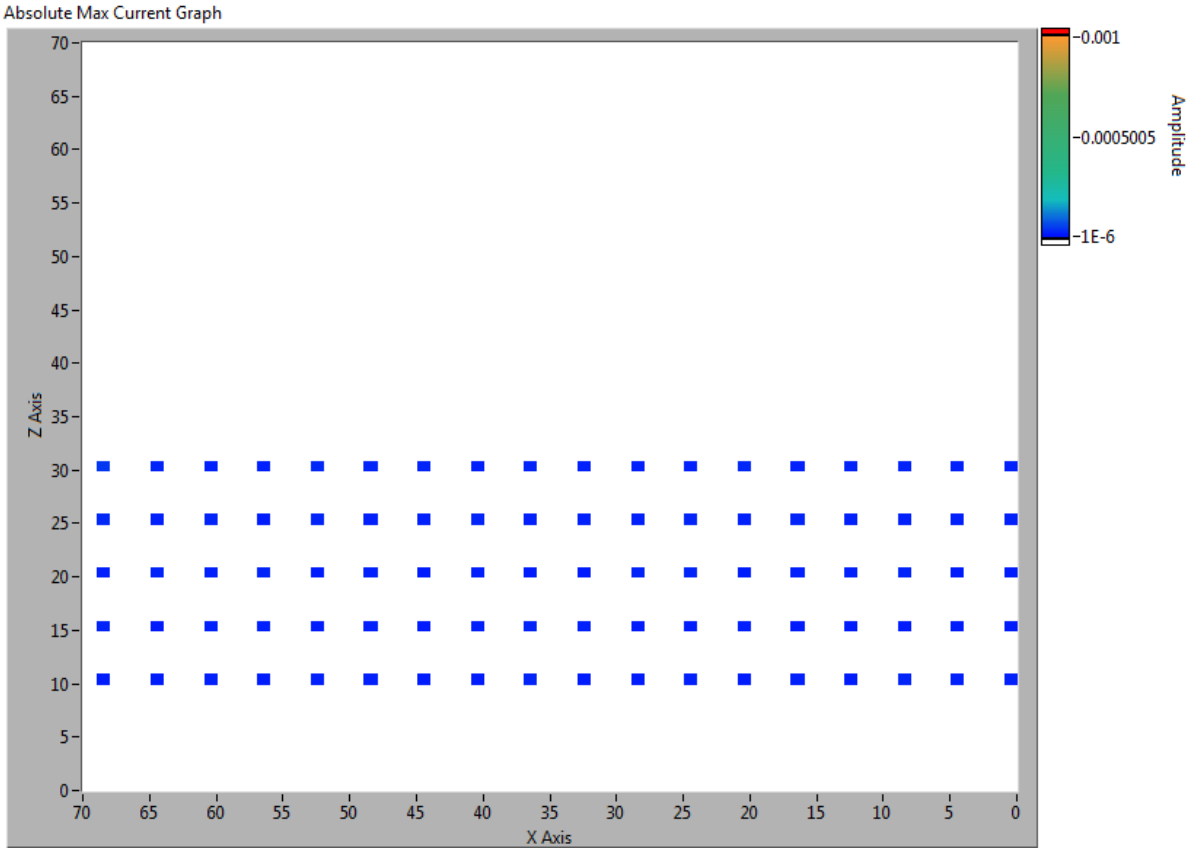

Figure 18: Color plot showing the absolute maximum current at each location when no material is present. Any resulting signal is due to electronic noise.

4. RESULTS – SPECIFIC CHEMICAL SYSTEMS

In order to draw conclusions on the photocatalytic activity of novel material spreads it is first necessary to decide how to digest and present the data. As stated in previous sections, there are several "factors of merit" that might be considered when looking to create an economical and practical solar energy technology. For this project we decided to look specifically at the maximum light induced current generated by different photon energy as well as the external voltage necessary to begin water decomposition. The two main visual representations of this data can be seen in Figure 19. Along with these charts, other charts may

be utilized to attempt to garner information on the activity of a selected material. Three color plots are used to show activity as a function of wafer position, 1) Absolute maximum current at each location, 2) The external potential at which this maximum current occurred, and 3) The current as a function of wafer position at a potential of 0 V.

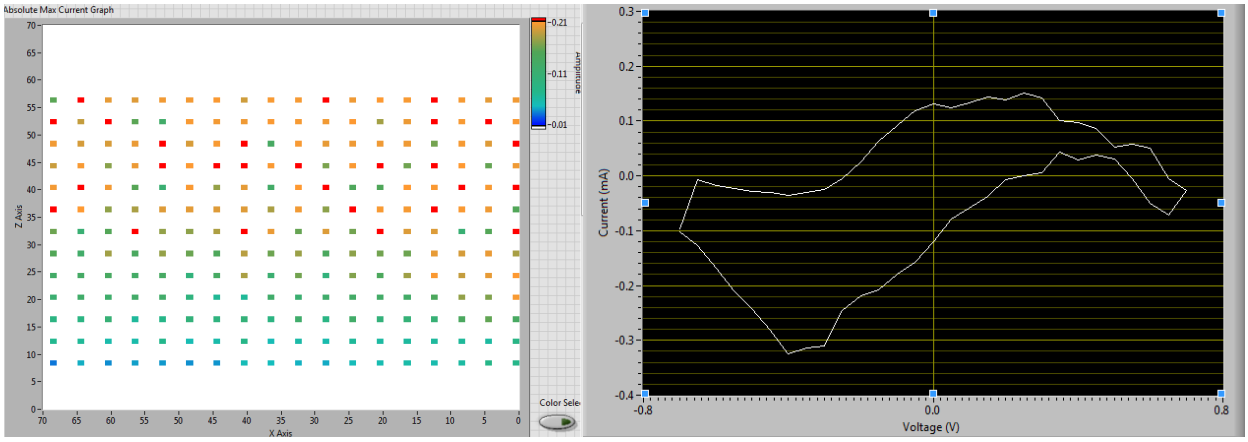

Figure 19: An example of the visual representations of the photocurrent data. LEFT: Color scale plot showing the absolute maximum current at each location as a function of wafer position. RIGHT: CV chart for a single wafer position showing the photocurrent as a function of the changing potential. In this example the -0.32 mA current at approximately -0.35 V would act as the "absolute maximum" current for this (x,z) location.

The nominal quantum yield was calculated based on the laser wavelength and power. The calculated quantum yield is only useful in comparing materials tested in this experimental setup because the calculation makes several gross assumptions including that the power and wavelength reported for each laser are accurate. Furthermore, although the soda-lime glass container does absorb more of the UV laser light than the green or red, and will have wavelength-dependent Fresnel reflections, absorption and reflection are completely neglected. With that in mind, the following calculations are used to determine the "relative" quantum yield.

$$E = \frac{hc}{\lambda} \quad (2)$$

where E represents the photon energy at wavelength λ with c and h representing the speed of light in vacuum and Plank's constant respectively. After determining the photon energy it is necessary to find the photon flux based on the power of the laser.

$$\Phi = \frac{P}{E} \quad (3)$$

Here Φ represents the number of photons per second leaving the laser. If the assumption is made that one photon will create one electron-hole pair that has no chance of recombination, this Φ represents the maximum photocurrent possible using that laser. Finally, determining the quantum yield of the material is a simple matter of dividing Φ by photocurrent measured during the experiment (I).

$$QY(\%) = \frac{I}{\Phi} \quad (4)$$

This simple quantum yield calculation was used for all three of the lasers utilized in the research. The resulting maximum values are given in Table 1:

Laser System	Wavelength (nm)	Rated Power (mW)	Φ (photons sec^{-1})	Maximum photocurrent (mA)
Metrologic HeNe	632.8	1	3.2E15	0.5
Wicked Lasers Core Series	532	5	1.3E16	2.1
Wicked Lasers E2 Series	405	25	5.7E16	8.2

Table 1: A comparison of the different laser systems and the maximum possible photocurrent generated.

A total of six material combinations were deposited using the technique discussed above. These materials were all sputtered at a base pressure of 30 mTorr with a 20% oxygen flow. Furthermore, all materials were sputtered with a substrate RF bias power sufficient to impart a dc potential of 75 volts on the substrate. The specific deposition conditions for each material spread are given in the following sections.

4.1 Ti-Ni-Co Oxide

Two Ti-Ni-Co wafers were the first to be tested. The known photoactivity of titanium oxide along with the reported catalytic properties of nickel and cobalt oxides motivated the choice of this combination. The deposition conditions for both wafers were as follows:

O_2 Partial Pressure = 20%

Ar Partial Pressure = 80%

Ti Magnetron Gun Power = 100 W

Ni Magnetron Gun Power = 100 W

Co Magnetron Gun Power = 100 W

Target Pre-sputter time = 10 min

Sputter Time = 40 min

The first wafer was tested without any post-deposition heat treatment. The titanium-rich region appeared to be relatively well oxidized while the nickel- and cobalt-rich regions were much more metallic. The wafer was tested in 0.5 M NaOH. Immediately upon contact with the

solution, the thin film peeled off the wafer along with the chrome and platinum under layers. Only a small are of the titanium-rich region remained but it was noticeably altered. The remaining film had cracks running through it as well as apparent rough patches.

A second Ti-Ni-Co wafer was then prepared. It was deposited in the same conditions as the first wafer but was then baked at 600 ^{o}C for 3 hours in air. The resulting oxide could not be tested as the heat treatment caused most of the film to peel, bubble, or crack. What was left of the film (as shown in Figure 20) was visibly more oxidized than before heat treatment but was unsuitable for photocatalytic testing. Based on this result it was decided that lower temperature post-sputter heat treatments would be used.

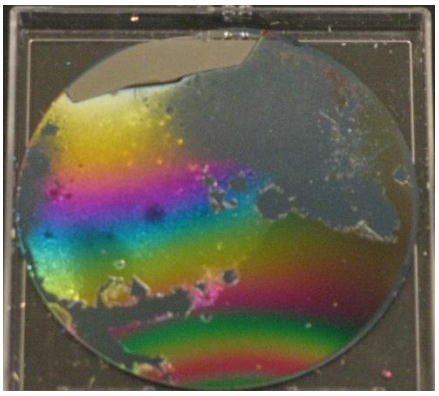

Figure 20: Photograph of Ti-Ni-Co wafer after 600 ^{o}C heat treatment for 3 hours.

4.2 Cu-Ni-Co Oxide

The Cu-Ni-Co-O wafer was prepared on a 3” silicon wafer as previously described. These three cations were chosen with the expectation that CuO_x could provide a light absorbing material with a bandgap suitable for photocatalysis while NiO_x and CoO_x might act as catalysts. The deposition conditions are as follows:

O_2 Partial Pressure = 20%

Ar Partial Pressure = 80%

Cu Magnetron Gun Power = 30 W

Ni Magnetron Gun Power = 100 W

Co Magnetron Gun Power = 100 W

Target Pre-sputter time = 10 min

Sputter Time = 40 min

After deposition the thin film was examined to determine the level of oxidation. The resulting thin film appeared almost entirely metallic. Only very slight coloration due to diffraction was observed on the Ni rich region of the wafer. In order to more fully oxidize the metals, the wafer was heated in air for 3 hours to 300 ^{o}C and later 450 ^{o}C. This heat treatment resulted in a more fully oxidized sample suitable for photocatalytic testing. A specular, rough area was observed after the heat treatment in the nickel rich region of the sample. Photographs of the progression of the wafer can be seen in Figure 21.

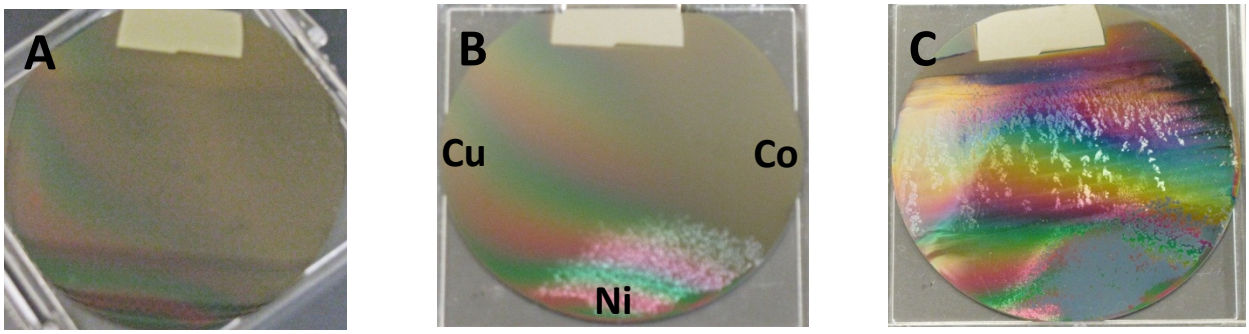

Figure 21: Photographs of the Cu-Ni-Co oxide films. **A.** Film after deposition and air bake at 300 ^{o}C for 3 hours. **B.** Film after subsequent 450 ^{o}C air bake. **C.** Film after full wafer test run in 0.1 M Na_2SO_4.

The wafer was tested in 0.1 M Na_2SO_4 with both the 405 and 532 nm lasers. Activity was measured on a 4mm square grid yielding 252 measurements for the 405 nm run and a 270 point grid for the 532 nm run. While the entire wafer could yield a maximum of 324 measurements at 4 mm centers, some reasons were not able to be tested due to mechanical constraints. Nevertheless, the area tested included all of the regions for which a single cation reaches its maximum concentration (i.e., the region closest to each respective sputter gun during deposition). The color plots below (Figure 22) represent the absolute maximum current observed for each of the two test runs. Both runs yielded similar maximum wafer currents of 7.3 µA and 7.95 µA for the 405 nm and 532 nm tests respectively.

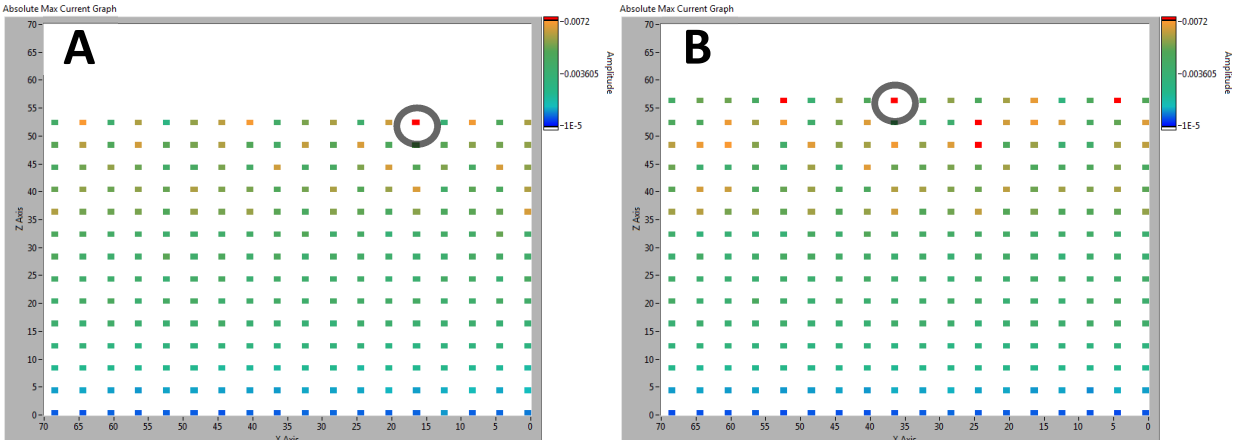

Figure 22: Color plots of the Cu-Ni-Co oxide films. **A.** Results of the 405 nm test. The maximum wafer current of 7.3 µA was obtained at (16,52). **B.** Results of the 532 nm test. The maximum wafer current of 7.95 µA was obtained at (36,56).

4.3 Ta-Ni-Co Oxide

The Ta-Ni-Co-O wafer was prepared using the same parameters as the previous. The Ta-O has shown some promise as a possible light absorbing material, so with this in mind it was

combined with two possible catalytic materials and tested under 405 nm and 532 nm irradiation. The specific deposition conditions are given below.

O_2 Partial Pressure = 20%

Ar Partial Pressure = 80%

Ta Magnetron Gun Power = 50 W

Ni Magnetron Gun Power = 100 W

Co Magnetron Gun Power = 100 W

Target Pre-sputter time = 40 min

Sputter Time = 40 min

After deposition it was once again inferred that the oxidation level was not sufficient to warrant tests. In order to oxidize the film, the wafer was heated in air to 300 ^{o}C for 3 hours followed by a subsequent 450 ^{o}C bake. After the 300 ^{o}C bake, interference was observed in the Ta-O rich region. The remaining portions of the wafer appeared metallic. After the 450 ^{o}C bake both the Ta and Ni rich regions showed strong interference colors while the Co rich region still appeared metallic. This is due to the fact that it is Co is less oxyphilic than Ta or Ni. Overall, it was decided that the resultant oxide layer was suitable for photocatalytic testing. Photographs of the resulting films can be seen in Figure 23.

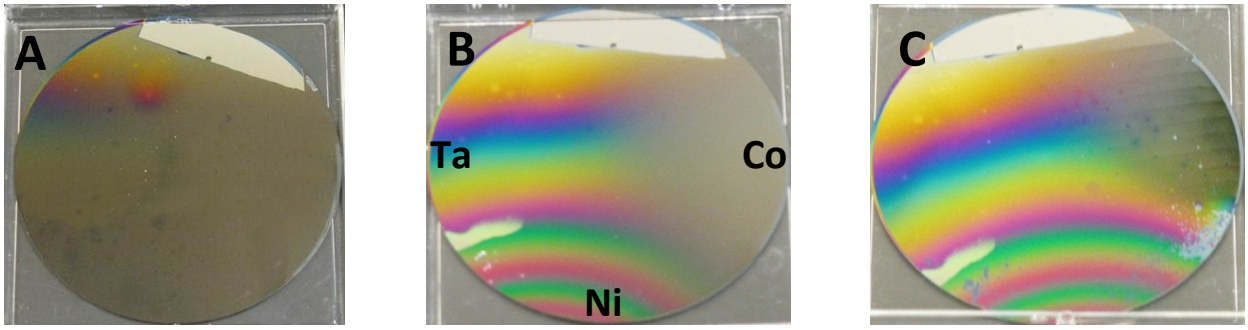

Figure 23: Photographs of the Ta-Ni-Co oxide films. **A.** Film after deposition and air bake at 300 ^{o}C for 3 hours. **B.** Film after subsequent 450 ^{o}C air bake. **C.** Film after full wafer test run in 0.1 M Na_2SO_4.

As with the Cu-Ni-Co film, the Ta-Ni-Co oxide wafer was tested in the electrochemical test cell. The wafer was tested on a square grid with 4 mm centers, with both the 405 and 532 nm lasers. The resulting color plots are shown in Figure 24.

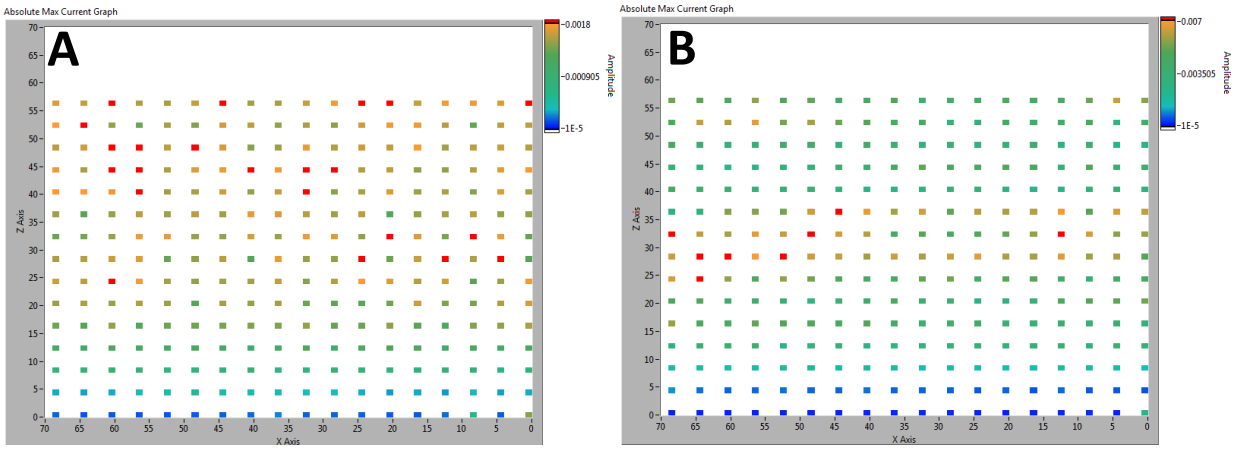

Figure 24: Color plots of the Ta-Ni-Co oxide films. **A.** Results of the 405 nm test. The maximum wafer current of 2 µA. **B.** Results of the 532 nm test. The maximum wafer current of 8.6 µA. Note the localized active areas of the 532 nm run.

The 405 nm test resulted in a very low, decentralized overall signal. While the maximum wafer current reached approximately 2 µA, it did not appear to correspond to any specific material combination. The 532 nm however, did show localized activity. Specifically, high

current, maxing out at 8.6 μA, was centered on the Co rich region. This result also suggested the role Ni may play as a possible catalyst. The high activity falls off as the laser is scanned over similar Ta-Co compositions with either higher or lower Ni levels. This suggests a specific composition or phase that is created in this area that is highly dependent on the material ratios.

While the 532 nm test did show localized catalytic activity, several questions remain. Specifically, more investigation is needed to characterize the composition and surface roughness in order to specifically determine the outer bounds of the high activity. Once the area of high activity is identified and characterized, it may be necessary to create a single composition sample in order to more accurately determine the photocatalytic properties.

4.4 Other Material Combinations

The final three material combinations were deposited in the same fashion as the previous wafers. The specific deposition parameters are outlined in Table 2:

Material Combinations	Cu-Ti-Co Oxide	Cu-Ni-Ta Oxide	Cu-Fe-Ni Oxide
O_2 Partial Pressure	20%	20%	20%
Gun 1 Power	30 W	30 W	100 W
Gun 2 Power	100 W	100 W	100 W
Gun 3 Power	100 W	100 W	100 W
Pre-Sputter Time	15 min	10 min	15 min
Sputter Time	40 min	40 min	40 min

Table 2: The sputtering conditions for the Cu-Ti-Co oxide, Cu-Ni-Ta oxide and Cu-Fe-Ni oxide films.

While the photocatalytic test results of these materials are not yet available, photographs of the wafers after deposition, heat processing, and test electrochemical runs can be seen below in Figures 25, 26, and 27.

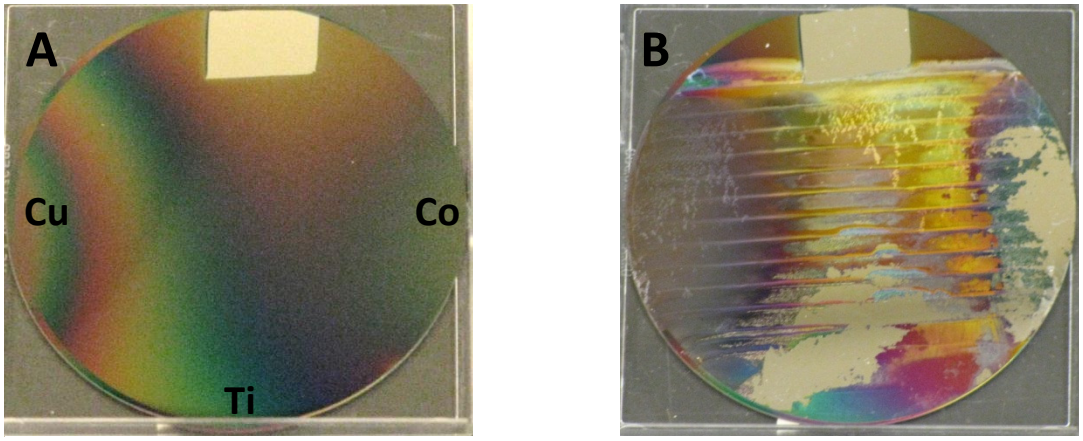

Figure 25: Photographs of the Cu-Ti-Co oxide films. **A.** Film after deposition and air bake at 300 ^{o}C for 3 hours. **B.** Film after prolonged submersion in 0.1 M Na_2SO_4.

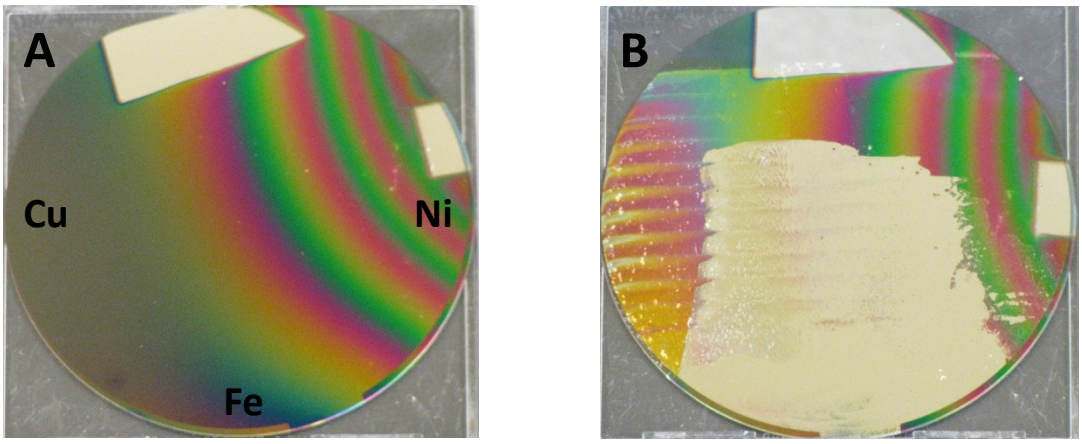

Figure 26: Photographs of the Cu-Fe-Ni oxide films. **A.** Film after deposition and air bake at 300 ^{o}C for 3 hours. **B.** Film after prolonged submersion in 0.1 M Na_2SO_4.

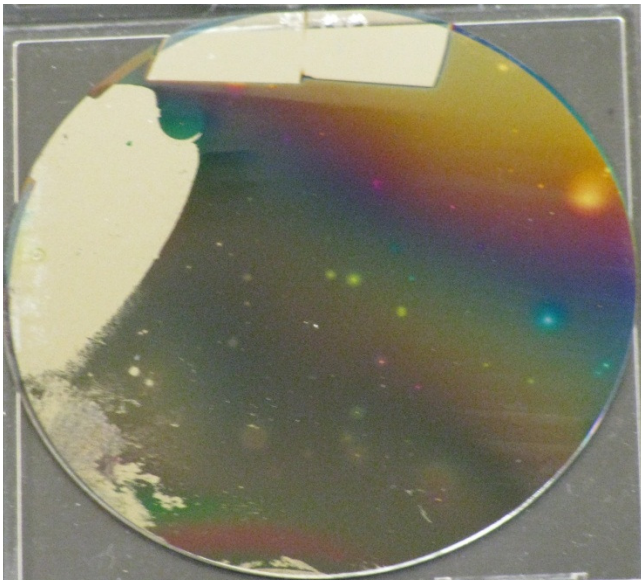

Figure 27: Photographs of the Cu-Ni-Ta oxide films after deposition, 300 ^{o}C air bake for 3 hours and electrochemical test run in 0.1 M Na_2SO_4.

It is worth noting the horizontal lines visible on all three wafers but highly visible on the Cu-Ti-Co-O and Cu-Fe-Ni-O films. This is believed to be caused by the interface between air and

the solution as the wafer is slowly lowered into the electrochemical cell. The meniscus that is formed at this interface creates a high potential region due to the very low amount of liquid at these locations. This accounts for the etching observed at 4 mm increments.

5. CONCLUSION

This research project primarily consisted of designing, building, testing, and optimizing an electrochemical system to test combinatorial material spreads for possible photocatalytic water splitting properties. The test system was specifically designed to move a 3" diameter wafer coated with a thin-film composition spread through an electrochemical cell and to observe any current produced by shining lasers of multiple wavelengths onto different locations on the wafer. A chopper system was used to perform a background subtraction calculation by looking at the difference between the current produced when the laser was allowed to reach the material wafer and any background current observed when the beam was blocked.

Once the measurement system was constructed and tested, six different oxide composition spreads were created using reactive magnetron co-sputtering. The material combinations were then tested for catalytic activity and were characterized based on their photoresponse as well as their stability in an aqueous environment. It was found that certain locations on the Cu-Ni-Co oxide films showed photocatalytic activity under both 405 nm and 532 nm radiation. The Ta-Ni-Co oxide films also showed some activity including a specific, high current region on the 532 nm test. This localized, Co rich region provided several high current measurements with a maximum value of just over 8.6 μA. The four remaining material oxide

spreads (Ti-Ni-Co, Cu-Ti-Co, Cu-Fe-Ni, and Cu-Ni-Ta) showed varying levels of stability under the aqueous conditions and will require further research to determine if the compositions in question can be tested.

Furthermore, a method of choosing novel material combinations for photocatalytic research has been developed.

In order to provide a benchmark reference, it is useful to compare the observed results to both theoretical and state-of-the-art photocatalytic materials. The higher current (8.2 μA on the Ta-Ni-Co oxide wafer) was observed using the 532 nm laser. A theoretical QY calculation shows that less than 0.4% of the available photons are able to create an electron-hole pair capable of splitting the water. If implemented in a real photocatalytic system, a one square meter system would be able to generate approximately 210 mW. Even other known visible light photocatalysts such as $(Ga_{0.88}Zn_{0.12})(N_{0.88}O_{0.12})$ (bandgap of approximately 2.9 eV) provide a QY of 5.9%; more than 10x the QY of the current Ta-Ni-Co sample.

6. FUTURE CONSIDERATIONS

Many significant issues were identified and resolved during the course of this research. As in any research, however, more questions have been raised than answered. Clearly, in order to gain a more complete understanding of the role different materials play on the properties of a combinatorial photocatalyst, it is necessary to test a much larger cross section of the periodic table. I suggest moving away from the transition metal region and incorporating rare earth metals and/or alkali and alkaline earth metals.

The ability to plot photocurrent as a function of wafer position, while informative, does not provide the full picture necessary to definitively identify a material as photoactive. It is necessary to take this data and look at it in the context of the larger system such as looking at the SNR and onset potential and the specified location. Furthermore, the materials absorption length should be determined in order to identify the percentage of incident photons absorbed within the thickness. This would provide a means of normalizing the efficiency across different material compositions.

While the goal was to choose magnetron gun powers such that the ternary material spread reached a 1:1:1 ratio near the center of the wafer, this has not been quantitatively verified by composition measurements. Work must be done to tune the gun powers for each material sputtered. A crystal monitor could be used to determine the relationship between gun power and deposition rate. Once this has been accomplished for all of the desired materials, the sputter rates may be chosen in order to provide a precise 1:1:1 ratio at the center; or any other desired ratio.

Furthermore, the effect of band engineering and the possibility it holds for new, more efficient photocatalysts is known but has not been explored in enough detail. Oxide materials must be compared quantitatively to their oxy-nitride counterparts in order to determine if the inclusion of nitrogen can provide a useful advantage over pure oxide materials. This process includes determining the exact percentage of nitrogen in an oxy-nitride material and

determining the relationship between percent nitrogen and change in valence band location. This can be done by characterizing similar oxide and oxy-nitride systems and comparing the differences. It would then be pertinent to determine the structure, crystallinity, as well as other relative information in order to determine the exact effect nitrogen incorporation has on the bandgap and photoactivity of the material.

While the experimental setup was sufficient for the tests desired, several improvements may be made in the future. First, although the rated laser power is known, the effect of Fresnel reflections on the beam has not been modeled. Measuring the laser power incident on the sample could be accomplished by using a calibrated thermopile detector. However, the effect of reflections at the air/glass, glass/solution, and solution/oxide film interfaces will still need to be modeled. This will require at least approximate values for the wavelength-dependent index of refraction of the oxide film as a function of material composition.

Secondly, the electrochemical portion of the experimental apparatus should be optimized to avoid the meniscus effects observed on several of the tested wafers. As this is a result of an increased localized potential at the air/solution/oxide film interface, it may be useful to rearrange the system wherein the wafer would be fully immersed at all times. This could be accomplished by either utilizing a larger, transparent container for the electrochemical measurements in which the material wafer would be moved with respect to the laser while staying fully submerged, or by submerging and fixing the position of the wafer while moving the laser. In either scenario, steps would need to be taken in order to isolate the electrical

connection between the wafer and potentiostat. It may also be useful to change the electrolyte or include a pH buffer in order to provide the most stable and catalytically favorable electrochemical conditions.

7. REFERENCES

[1] THORLABS apt™ Stepper Motor Controllers, http://thorlabs.com/NewGroupPage9.cfm?ObjectGroup_ID=1704

[2] THORLABS 150 mm Linear Travel Solutions, http://thorlabs.com/NewGroupPage9.cfm?ObjectGroup_ID=2132

[3] Wicked Lasers Core Series, http://wickedlasers.com/lasers/Core_Series-67-3.html

[4] Stanford Research Systems Optical Chopper, http://www.thinksrs.com/products/SR540.htm

[5] Electromagnetic Spectrum, http://hyperphysics.phy-astr.gsu.edu/hbase/ems3.html

[6] Jos Oudenhoven, Freek Scheijen, Martin Wolffs, Hans Niemantsverdriet. "Fundementals of Photocatalytic Water Splitting by Visible Light", 21-April-2004

[7] *Michael Grätzel. "Photoelectrochemical Cells" Nature* **414**, 338-344 (15 November 2001)

[8] Eric D. Cline, Stefan Bernhard. "The Transformation and Storage of Solar Energy: Progress Towards Visible-Light Induced Water Splitting", CHIMA **2009**, 63, No. 11

[9] Akihiko Kudo. "Photocatalysts and solar hydrogen production", *Pure Appl. Chem.*, Vol. 79, No. 11, pp. 1917–1927, 2007.

[10] Newport Introduction to Solar Radiation, http://www.newport.com/Introduction-to-Solar-Radiation/411919/1033/content.aspx

[11] Akira Fujishima, Kenichi Honda. "Electrochemical Photolysis of Water at a Semiconductor Electrode", Nature 238 (1972) 37

[12] Kazuhiko Maeda, Kazunari Domen. "Photocatalytic Water Splitting: Recent Progress and Future Challenges", J. Phys. Chem. Lett. 2010, 1, 2655–2661

[13] Asif Khan. “Device Physics: A bug-beating diode”, *Nature* **441**, 299(18 May 2006)

[14] Akihiko Kudo, Yugo Miseki. “Heterogeneous photocatalyst materials for water splitting”, Chem. Soc. Rev., 2009, 38, 253–278 | 253

[15] Michael Woodhouse, G. S. Herman, B. A. Parkinson. “Combinatorial Approach to Identification of Catalysts for the Photoelectrolysis of Water”, Chem. Mater. **2005,** 17, 4318-4324

[16] Yanfa Yan. “Metal-oxide bandgap engineering for photo-electrochemical water splitting”, 3 November 2010, SPIE Newsroom

[17] J. Choi, R. Puthenkovilakam, J. P. Chang. “Effect of nitrogen on the electronic properties of hafnium oxynitrides”, JOURNAL OF APPLIED PHYSICS **99**, 053705 (2006)

[18] Fahri Uslu. “Structural and optical properties of copper- and nickel-oxynitride films”

[19] R Bruce van Dover. “high-throughput experimental techniques: inorganic thin films: dielectrics and electrocatalysts”, Department of Materials Science and Engineering, Cornell University

[20] Seung Bin Park. “Photocatalytic water splitting”, http://web.kaist.ac.kr/~lamp/research.html

[21] Jeon G. Han. “Magnetron Sputtering Technology”, Center for Advanced Plasma Surface Technology (CAPST). Sungkyunkwan University

[22] Institute of Materials & Machine Mechanics. Slovak Academy of Sciences, “PVD – physical vapor deposition”, http://www.umms.sav.sk/index.php?ID=415

[23] Brigham Young University. “Oxide Growth Calculation”, http://www.cleanroom.byu.edu/OxideThickCalc.phtml

[24] Brewton-Parker College. “ History of the Development of the Periodic Table of Elements”, www.bpc.edu/mathscience/chemistry/history_of_the_periodic_table.html